Two-dimensional imaging of thermal diffusivity in metals by scanning photodeflection detection

Ulises Crossa Archiopoli,[1] Nélida Mingolo,[1,a)] and Oscar E. Martínez[2,3]
[1]*Dto. Física, Facultad de Ingeniería, Universidad de Buenos Aires, 1428 Buenos Aires, Argentina*
[2]*Dto. Física, Facultad de Ciencias Exactas, Universidad de Buenos Aires, 1063 Buenos Aires, Argentina*
[3]*CONICET, Rivadavia 1917, 1203 Buenos Aires, Argentina*

(Received 15 August 2009; accepted 9 December 2009; published online 27 January 2010)

We present a technique that retrieves the thermal diffusivity of metallic samples in a two-dimensional map with micrometer resolution. The technique uses a photothermal method based on the deflection of a probe beam after heating the surface with a modulated pump. After adequate calibration, the time delay between the pump modulation and the deflection modulation provides direct information on the local thermal diffusivity. The calibration is carried out by measuring the frequency dependence of the deflection signal at several sample locations. The capabilities of the technique are illustrated with the measurement of a cross section of a surface treated steel sample.
 [doi:10.1063/1.3289218]

I. INTRODUCTION

The properties of a metallic material depend strongly not only on its composition but mostly on the particular phases present in the microstructure. Hence identifying the phase distribution has been a permanent task originally performed qualitatively by metallographic inspection with selective etching and, more recently in a more quantitative manner, by microscopic scanning techniques based on the electron microscope. For phases of different compositions energy dispersive spectroscopy techniques might be sufficient, while phases of similar chemical compositions require more elaborate methods such as electron back-scattering diffraction.[1]

In this work, we present an alternative technique that allows a rapid determination of the thermal diffusivity at a micrometer level, a thermal property that strongly depends on the crystallographic structure, and thus allowing the distinction, even for phases with very similar chemical composition. The technique relies in the determination of the photothermal deflection of a probe beam due to the deformation of the surface because of the modulated heating from a pump beam. Standard photothermal techniques rely in the determination of the spatial delay of the signal as a function of the separation between the pump and probe beams,[2–8] or else in the frequency dependence at constant separation.[7–12] We show in this work that the information can be retrieved by a single determination of the phase delay between the pump and probe modulations at constant frequency, while the surface is scanned to retrieve a two-dimensional (2D) map of the thermal diffusivity. The resolution depends on the modulating frequency and beam sizes.

In Sec. II, a description of the photothermal technique is presented. The sample preparation and characterization are described in Sec. III, and the results and discussions are presented in Sec. IV. The final conclusions are presented in Sec. V.

[a)]Electronic mail: nmingol@fi.uba.ar.

II. THE PHOTOTHERMAL TECHNIQUE

The technique used is based on a modified version of the method reported before,[12] consisting on the heating of the surface by a modulated laser beam, the simultaneous detection of the change in reflectance,[4–7] and the deflection of the probe beam.[10,11] The change in the reflectance is due to the temperature rise and the deflection arises from the surface deformation caused by the localized thermal expansion, as described in Fig. 1. The deflection is sensed by intercepting part of the beam with a knife edge, generating in this manner a modulation of the detected signal as the beam oscillates laterally.

As shown in Ref. 12, the detected signal (modulated component of the reflected probe) can be written as

$$S_\omega = Af(\omega/\omega_0, N, \xi_P', \eta_P') + Bg(\omega/\omega_0, N, \xi_P', \eta_P') \tag{1}$$

with

$$A = P_P \tau(0, x_K) \frac{dR}{dT} \frac{(1-R')}{\sqrt{2} 4\pi^2 \kappa_r} P_\omega \sqrt{\frac{D_r}{D_z}} \frac{1}{\sqrt{\sigma_\xi \sigma_\eta}}, \tag{2}$$

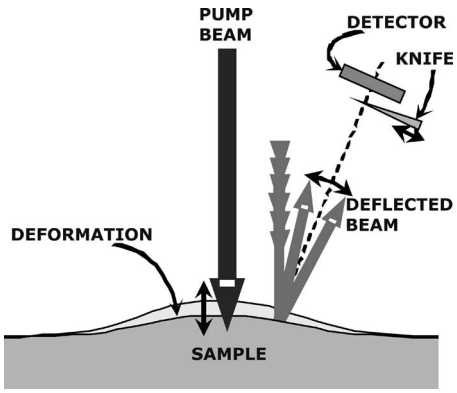

FIG. 1. Schematics of the mechanisms giving rise to the signal. The surface deformation deflects the probe beam that is partially clipped by the knife edge before reaching the detector. The change in reflectivity with temperature also contributes to the signal.

TABLE I. Glossary of terms.

S_ω	Signal detected at frequency ω
D_r	Thermal diffusivity parallel to the surface
D_z	Thermal diffusivity perpendicular to the surface
λ_z	Thermal expansion in the z direction
κ_r	Thermal conductivity parallel to the surface
ω	Modulation frequency
$\omega_o=2\pi f_0$	Characteristic frequency
R	Reflectivity of the sample at the probe wavelength
R'	Reflectivity of the sample at the pump wavelength
ξ, η	Coordinates along the principal axis of the pump ellipse
σ_ξ, σ_η	Incident spot size along the coordinates ξ and η
$N=\sigma_\xi/\sigma_\eta$	Aspect ratio of the beam
ξ_P', η_P'	Normalized coordinates of the probe beam respect to the pump beam center.
x_b	Beam center position at the knife edge plane
x_K	Knife edge position
P_ω	Modulation depth of the pump power
P_p	Probe beam power
τ	Transmission of the optical system between the sample and the detector
z_f	Focal distance of the objective
λ	Pump beam wavelength
λ_P	Probe beam wavelength
σ_P	Probe beam size at the sample

$$B = P_P P_\omega R \left.\frac{d\tau}{dx_b}\right|_{x_b=0} \frac{z_f}{2\sigma_\xi}\frac{(1-R')}{\sqrt{2}\pi^2}\frac{\lambda_z}{\kappa_r}. \quad (3)$$

In Table I, a glossary of the terms used is presented. The term Af is the contribution from the change in reflectivity (photoreflectivity signal) and Bg is the contribution from the photodeflection signal. A and B are factors that depend on the material and beam size, while f and g are dimensionless functions that depend on the beam separation and on the material only through the critical frequency

$$\omega_0 = \frac{2D_r}{\sigma_\xi \sigma_\eta}. \quad (4)$$

It should be noticed that from Eq. (3) the amplitude of the photodeflection signal varies with the sample tilt as it would change the position of the center of the beam at the knife edge. To avoid any significant effect of surface undulations as the sample surface is scanned, the change in the tilt due to loss of planarity should be kept much smaller than the diffraction of the beam leaving the surface, i.e., much smaller than λ_P/σ_P. Nevertheless it must be noticed that the phase of the signal will not be affected by the tilt, and hence measurements relying only in the changes in the phase, as described below, will be insensitive to changes in the tilt.

From the fit of the measured signal by Eq. (1) and using A, B, and ω_0 as the adjustable parameters, the critical frequency and hence the in-plane thermal diffusivity D_r can be determined.

From Eqs. (1)–(3) it can be observed that the two terms that contribute to the signal have distinct frequency dependences. Hence, in order to retrieve the thermal diffusivity, the entire expression is fitted (as described in Ref. 12) after measuring the signal for a wide range of frequencies at least one decade above and below the critical frequency ω_0 defined in Eq. (4). But, if around the critical frequency one of the terms is significantly larger than the other one, then the expression can be approximated by the dominant term. The feasibility of this approximation will depend on the material properties and beam separation, as for example, for perfectly centered beams the deflection signal cancels. On the other hand, the photoreflectivity signal depends on the particular wavelength used for the probe beam and eventually can be selected such that this contribution becomes negligible for particular materials.

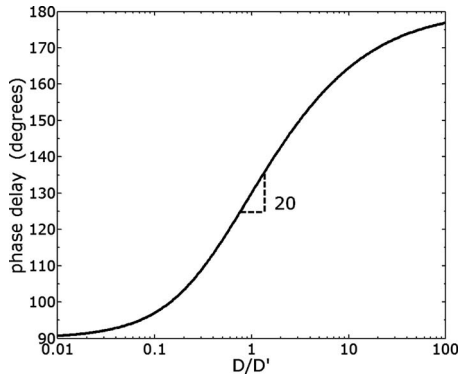

FIG. 2. Dependence of the phase delay with the normalized thermal diffusivity when only the photodeflection term is significant. The maximum slope of about 20 is observed around $D/D'=1$.

For many materials one of the terms of Eq. (1) is much larger than the other one. For the case of steel samples the dominant term is the photodeflection signal. In this case the phase of the complex signal depends only on the arguments of the function g in Eq. (1). If the thermoreflectance term is dominant, the argument of the function f will determine the phase. Such arguments are only the beam sizes, shapes and separations, the modulating frequency, and the thermal diffusivity (the only sample dependent coefficient). If the beams and modulating frequency are kept constant while scanning, the change in the phase of the signal can only arise from a change in the thermal diffusivity. This fact can then be used in order to retrieve the in-plane thermal diffusivity by only measuring the phase delay at constant frequency, provided that the beam sizes and separations are also kept constant.

In Fig. 2 the phase delay is plotted as a function of the thermal diffusivity, normalized to the diffusivity D' defined as the value of the diffusivity that yields a critical frequency ω_0 equal to the modulating frequency ω. The slope of 20 at $D/D'=1$ means that a 5% change in the diffusivity yields a change of one degree in the phase delay. This large sensitivity is found almost one decade above and below that critical diffusivity D'. Hence by scanning the sample while measuring the phase delay it should be possible to map the thermal diffusivity variations with very high sensitivity.

III. EXPERIMENTAL SETUP

The experimental setup is shown in Fig. 3. A pump laser emitting at $\lambda=532$ nm is modulated at the desired frequency

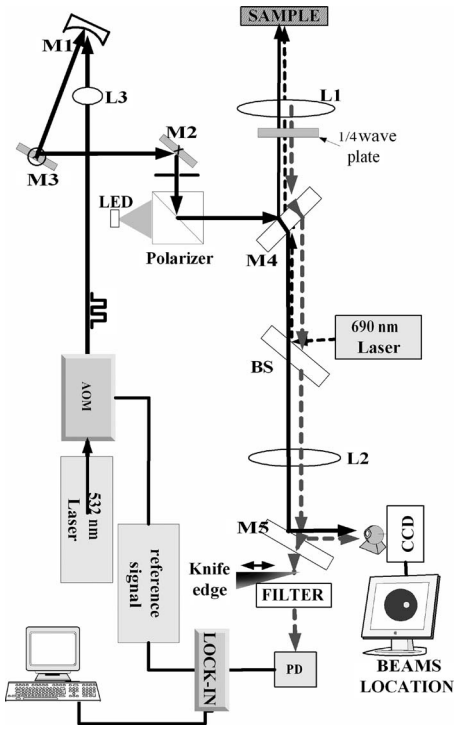

FIG. 3. Experimental setup. An AOM chops the green pump beam at the desired frequency. The reflected red signal is partially clipped by the knife edge and collected by the PD. The CCD allows the beams position and size measurement. L: lenses and M: mirrors. L1 is a microscope objective. A LED is included to illuminate the sample and register with the CCD an optical image of the analyzed region.

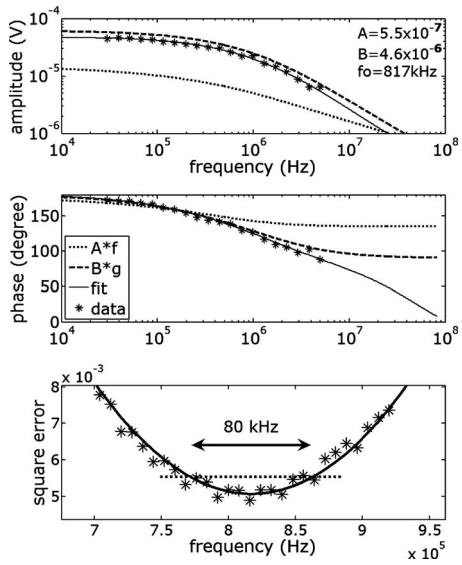

FIG. 4. Example of one measurement and fit. The measured signal is fitted by the functions accounting for the two contributions, the photoreflectivity $Af(\omega)$ and the photodeflection $Bg(\omega)$.The text box is common to (a) and (b) and shows the values of the least square fit. (a) Amplitude, (b) phase angle, and (c) square error as a function of the fitting critical frequency. This curve is used in order to determine the uncertainty in the fit.

(between 30 kHz and 5 MHz) and is focused on the sample surface by means of a microscope objective. A probe laser emitting at $\lambda=690$ nm is focused besides the pump about one spot size away and the reflection is detected by means of a photodiode (PD) after being clipped by the knife edge. Two objectives were used in the experiment, a 10× objective with a focal distance $z_f=20$ mm and a 4× objective with a focal distance of 45 mm. The 10× objective focused the beams to $\sigma=1.5$ μm, yielding a focal depth $2\pi\sigma^2/\lambda=26$ μm. The 4× objective focused the beams to $\sigma=3.4$ μm and the focal depth was 137 μm. The camera allows the precise focusing, the observation of the sample and the measurement of the beam size. The signal is filtered by a lock-in amplifier in order to extract the modulated component, both in amplitude and phase, at the pump beam modulation frequency.

The measured signal is corrected in order to account for the cross-talk between signal and reference channels in the high frequency lock-in amplifier (Stanford Research Instruments model SR844), and also the frequency response of the acousto-optic modulator (AOM) and the detector. The signal is fitted by Eq. (1) as described in detail in.[12]

In Fig. 4 one example of the fitting for one particular point at the sample is presented. The amplitude and phase are fitted [Figs. 4(a) and 4(b)] simultaneously and the fitting curve is superimposed with the experimental result. The factors Af and Bg are also shown to illustrate their different frequency dependence and relative weight. In the frequency range explored, the photodeflection mechanism (Bg) was always much larger than the photoreflectance one (Af). For each fitting frequency f_0 the parameters A and B are fitted by the least square method, following the procedure described in Ref. 12 and the error is plotted in order to determine the value of f_0 and its interval of confidence as shown in Fig. 4(c). Besides the uncertainty arising from the noise in the measurement and the quality of the fit there is an error source due to the error in the beam relative positions and the beam sizes [see Eqs. (1) and (4)]. Propagating these errors showed that they give rise to a negligible contribution to the critical frequency determination, as compared to the fitting error source described before.

The plot of the phase delay as a function of frequency in Fig. 4(b) shows the distinct behavior of the two mechanisms. But it also shows that for this sample the photodeflection mechanism is dominant. Hence neglecting the photoreflectance contribution, the measurement of the phase delay at a fixed frequency can be used in order to retrieve the thermal diffusivity.

IV. SAMPLE PREPARATION AND CHARACTERIZATION

The method was tested in a surface treated steel alloy. The bulk sample (AISI 4140) was surface treated by single shot with a cold cathode electron gun.[13–16] It has been shown previously[17,18] that this technique transforms a layer of a few microns thick to a metaestable phase. The gun consists of a pulsed glow discharge developed after establishing a high voltage at the cathode by means of a spark gap switch. Using a source voltage of 17 kV, the current pulse width was 20 μs, the peak current 21 A and the beam area at the sample location was 10 mm^2.

The rapid heating of the surface due to the electron bombardment creates a melt pool several microns thick, that rapidly cools dissipating the heat against the substrate. The cooling rate computed from the simulations is above 10^8 K/s at

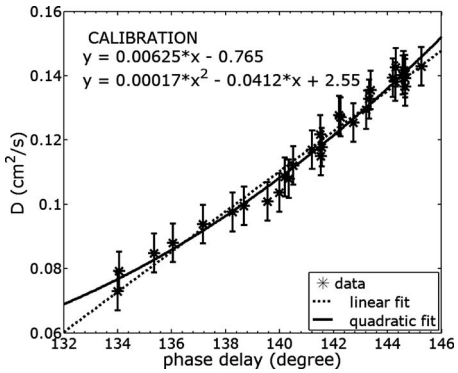

FIG. 5. Plot of the thermal diffusivity as a function of the phase delay at a fixed frequency of 150 kHz for a line scan across the treated area. The linear and quadratic fits to the data are also shown. Fit: x and y denote the phase delay and the diffusivity, respectively.

the beam center. The different durations of the melted pool yield different textures. The roughened surface appears due to Bènard–Marangoni instability[18] and has been shown to require a certain time to develop. Grazing incidence x-ray diffraction showed an important martensite content (48 vol %), a similar content of ferrite (45 vol %) and a minor amount of retained austenite (5 vol %) and F_3C (2 vol %). The treated region is several micrometers deep.[19]

For the cross section measurements, special care had to be taken to keep the treated area under study plane enough to be in focus during the entire scan. Besides, as mentioned before, it is convenient to keep the changes in the tilt angle as low as possible during the sample scan. When polishing the planarity is always lost toward the borders of the sample, that result rounded. To shift the border away from the treated area, before cutting, the sample was coated with a layer of electrodeposited nickel about 10 μm thick. The sample was also encapsulated in an acrylic matrix.

V. RESULTS AND DISCUSSIONS

The sample was scanned along a line in the cross section for the measurement of the thermal diffusivity. A spatial scan across the treated area was performed taking a full frequency scan from 30 kHz to 5 MHz. The result was used to retrieve the thermal diffusivity as a function of the position. With the same spatial scan the phase delay between the modulated pump and the signal was determined at a fixed frequency of 150 kHz, a value very close to the critical frequency for the base material for the objective used (4×). To compare the two methods, thermal diffusivity and phase delay are plotted in Fig. 5. The curve was fitted linearly and quadratically showing that although a linear fit would be enough for an adequate retrieval of the thermal diffusivity from the phase delay, the quadratic fit is more accurate. This occurs because the frequency selected is not necessarily exactly at the average critical frequency where the second order term would vanish (as seen in Fig. 2). The calibration parameters depend on the beam sizes and separation and hence should be recalculated when any of this parameters changes.

Finally the procedure was repeated for a new line and a full 2D scan with a higher magnification (10× objective). A new calibration was performed using complete scans of the

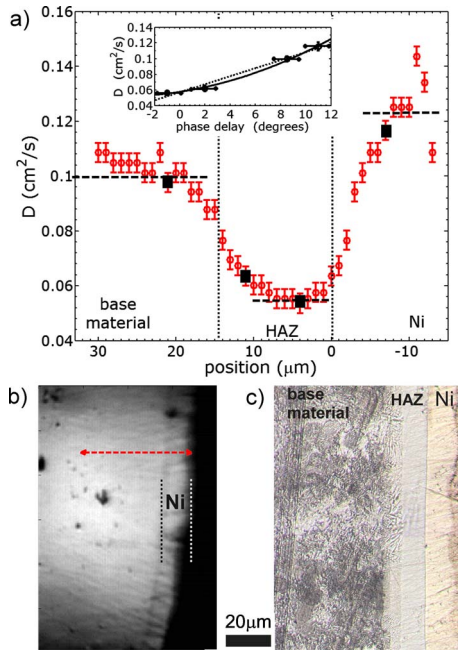

FIG. 6. (Color online) (a) Thermal diffusivity as a function of the position for a cross section. Inset: calibration curve, (b) optical micrograph recorded by the CCD camera, indicating the scanned region in the sample, and (c) optical micrograph for the etched sample, the base material structure (pearlite) is revealed.

photothermal signal as a function of the frequency at four representative points, one in the Ni layer, two in the heat affected zone (HAZ), and one in the base material [Fig. 6(b)]. All curves were fitted with the procedure described before and the thermal diffusivity was retrieved. With these four points the calibration curve shown in the inset of Fig. 6(a) was obtained for the thermal diffusivity as a function of the phase delay for a fixed frequency of 700 kHz. The frequency was larger than the selected with the 4× objective, in order to compensate for the increase in the critical frequency with the reduction in the beam area [Eq. (4)].

Using this calibration a measurement along a line with 1 μm steps was performed at constant frequency and registering the phase delay. The result of the retrieved diffusivity is shown in Fig. 6 together with a micrograph of the scanned cross section, taken with the charge-coupled device (CCD) camera [Fig. 6(b)]. The Ni layer can be recognized but the micrograph taken through the same objective does not show any structure in the treated material, since no etch was performed to reveal structures. The same sample was etched to reveal the characteristic pearlite structure as described in Ref. 19 [Fig. 6(c)]. The microstructure of base material can be observed but the central melted region of the sample appears as a continuous layer over the substrate (not revealed by etching).

The objective focused the pump beam to a 3 μm beam diameter at the sample location. As the beam is scanned across the border between the nickel layer and the treated material the diffusivity decays from the value of $D = 0.114 \pm 0.018$ cm^2/s (typical for this ferritic steel[20]) to a value of $D = 0.057 \pm 0.003$ cm^2/s (typical for the hardened martensitic steel layer.[21] The smooth transition from Ni to

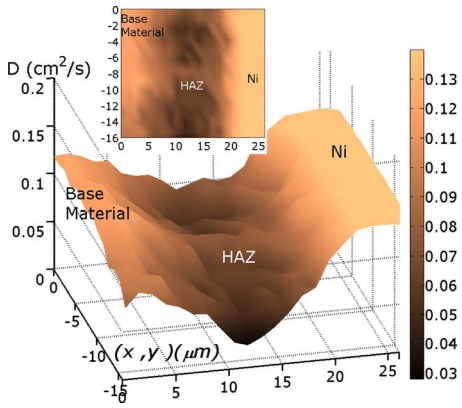

FIG. 7. (Color online) Thermal diffusivity vs position for the scanned area shown in a 3D plot. Inset: corresponding 2D map for the same data.

HAZ is due to the beam size, which averages over a region 3 μm wide. Another transition is observed between the hardened layer and the base material. This transition is smoother than the one between the Ni and the HAZ and is not an artifact due to the beam size but an indication of gradual changes in the material properties.

The good correlation between phase delay at a fixed frequency and thermal diffusivity in steel treated samples allows the determination of the structural changes in the field of view while minimizing the time consumed in the measurement.

Following the same procedure but now scanning the laser beams instead of the sample holder, by means of two rotating motors mounted as to tilt the beam along two perpendicular axes, a 2D image of the phase delay can be measured. Using the calibration curve, the map of the thermal diffusivity, and hence of the crystalline phases present in the treated structure, is retrieved. This is shown in Fig. 7, where not only the Ni layer can be clearly distinguished but also the hardened surface layer and the transition toward the untreated base material as the beam scans inward in the sample cross section.

It is worthwhile mentioning that for our sample the technique could not resolve the lamellar structure of the pearlite [see Fig. 6(c)]. If beam sizes smaller than the microstructure features were used, the technique might provide information on such structure.

If higher resolution is desired, the beam size can be reduced keeping in mind that the modulating frequency should be scaled as indicated by Eq. (4), i.e., quadratically with the beam size. It should also be noticed that the two described mechanisms, photoreflectivity and photodeflection, scale inversely with beam size [Eqs. (2) and (3)] but the photodeflection signal also scales with the objective focal distance z_f. Hence if the beam is reduced by changing the objective the parameter A will grow while the parameter B will remain constant, and the assumption of $B \gg A$ might no longer be valid. This can be tested for each sample and focusing condition when performing the calibration curves (full frequency scans) at selected points.

VI. CONCLUSIONS

A rapid technique has been presented that allows the determination of the thermal diffusivity of metallic samples with microscopic spatial resolution. The technique is based on a photothermal technique that uses the simultaneous determination of the photoreflectance and the photodeflection. In contrast to prior implementations it was shown that, after adequate calibration, the time delay between the pump modulation and the deflection modulation provides direct information on the local thermal diffusivity. This reduces the time consuming scans of an additional magnitude such as the frequency of modulation or the pump and probe beam separation. This simplification is possible if only one of the contributions to the signal is dominant, and for the particular case used in this work it was the deflection signal that was much higher than the thermoreflectance signal.

The calibration was performed by making full scans over two decades of the signal as a function of the frequency, but only for four points of the scanned area. After such calibration and as long as the beam sizes and relative distances remain constant, the determination of the phase delay at a fixed frequency was proved to be sufficient for the retrieval of the thermal diffusivity in the entire scanned area. A one degree error in the phase delay resulted in a 5% error in the thermal diffusivity measurement, showing a very high contrast capability for phase discrimination, as for example, the thermal diffusivity between a martensite and a ferrite in steel of the same composition differs by a factor of two.

The technique was tested in the characterization of a cross section of a thermally treated surface of a steel alloy. The contrast resulted better than optical microscopic determinations (even when done with chemical etch of the sample) and the martensitic layer could be clearly distinguished from the base material, and moreover, the transition layer could be precisely characterized.

[1] A.F. Gourgues-Lorenzon, J. Microsc. **233**, 460 (2009).
[2] J. F. Bisson and D. Fournier, J. Appl. Phys. **84**, 38 (1998).
[3] A. M. Mansanares, T. Velinov, Z. Bozoki, D. Fournier, and A. C. Boccara, J. Appl. Phys. **75**, 3344 (1994).
[4] L. Bincheng, J. P. Roger, L. Pottier, and D. Fournier, J. Appl. Phys. **86**, 5314 (1999).
[5] D. Fournier, MRS Bull. **26**, 465 (2001).
[6] D. Rochais, H. Le Houëdec, F. Enguehard, J. Jumel, and F. Lepoutre, J. Phys. D **38**, 1498 (2005).
[7] A. Rosencwaig, J. Opsal, W. L. Smith, and D. L. Willenborg, Appl. Phys. Lett. **46**, 1013 (1985).
[8] C. Hu, J. Zhao, and J. Shen, Rev. Sci. Instrum. **74**, 459 (2003).
[9] F. B. G. Astrath, N. G. C. Astrath, J. Shen, J. Zhou, and M. L. Baesso, J. Appl. Phys. **104**, 066101 (2008).
[10] A. Rosencwaig, J. Opsal, and D. L. Willenborg, Appl. Phys. Lett. **43**, 166 (1983).
[11] J. Opsal, A. Rosencwaig, and D. L. Willenborg, Appl. Opt. **22**, 3169 (1983).
[12] O. E. Martínez, F. Balzarotti, and N. Mingolo, Appl. Phys. B: Lasers Opt. **90**, 69 (2008).
[13] Y. Cesa, N. Mingolo, and O. E. Martínez, IEEE Trans. Plasma Sci. **28**, 1035 (2000).
[14] N. Mingolo, Y. Cesa, O. E. Martínez, J. I. Etcheverry, and J. J. Rocca, IEEE Trans. Plasma Sci. **28**, 386 (2000).
[15] N. Mingolo, C. R. González, O. E. Martínez, and J. J. Rocca, J. Appl. Phys. **82**, 4118 (1997).
[16] P. M. Belçaguy, N. Mingolo, and O. E. Martínez, IEEE Trans. Plasma Sci.

31, 788 (2003).
[17]U. Crossa Archiopoli, N. Mingolo, and O. E. Martínez, Metall. Mater. Trans. A **36**, 999 (2005).
[18]N. Mingolo, A. N. Roviglione, and O. E. Martínez, J. Mater. Res. **16**, 2343 (2001).
[19]U. Crossa Archiopoli, N. Mingolo, and N. Mingolo, Surf. Coat. Technol. **202**, 5982 (2008).
[20]M. Bauccio, *ASM Metals Reference Book*, 3rd ed. (ASM International, Materials Park, 1993), pp. 300–305.
[21]http://www.matweb.com/